Second order, iterative least squares inversion of anacoustic reflections

Scott Keating and Kris Innanen

ABSTRACT

A second order, iterative least squares approach to anacoustic inversion is presented and tested. Results are compared to linearized inversions, and failure regions and their causes are explored. While the second order approach offers improvement over the linearized approach, problems associated with very low and high Q are caused by other factors and are not greatly improved by the second order inversion.

INTRODUCTION

Recovery of seismic attenuation attributes is a problem of interest in geophysics, and hydrocarbon exploration in particular. This is is due large part to the potential for detecting hydrocarbons by the change in attenuation properties they cause, and the associated frequency dependence (Castagna et al. (2003); Odebeatu (2006)). The problem of inversion for attenuation parameter Q has been approached in previous CREWES reports, both in anacoustic (Innanen (2011)) and anelastic formulations (Innanen (2012)). In Innanen (2011), second order approximations are developed to better recover velocity and attenuation as these terms grow larger. In Bird et al. (2011), problems in reliability and accuracy introduced by noise and deconvolution are addressed by solving an overdetermined system of equations for the perturbations by least squares. Unfortunately in order to make this problem strictly linear for a least squares solution, we forfeit the increased accuracy of the second order solution. To address this problem, we here demonstrate an iterative least squares approach to solving for the second order expression. This allows for a more accurate, robust solution.

Introducing an iterative approach to solving for model parameters allows us to deal with another problem. While ideally we do our inversion based on the complex reflection coefficient, this requires accurately recovering the real and imaginary parts of the Fourier transform of the reflection coefficients. In practice, with noisy data that contains a wavelet, it can be problematic to accurately recover the real and imaginary parts of this Fourier transform. The amplitude spectrum is far simpler to recover, so an approach that uses only the measured amplitude spectrum is preferable. As shown in Bird (2012), if the imaginary part of the reflection coefficient is much less than the real part, then the amplitude spectrum will approximate the real part of the reflection coefficient. However, using iterative updating, we can instead find an approximation of this real part by assuming a small, but non negligible imaginary part.

SECOND ORDER, ITERATIVE LEAST SQUARES INVERSION

From Innanen (2011), we see that the expression for the anacoustic reflection coefficient is

$$R(\omega, \theta) = \frac{c\,\cos\theta - c_0[1 + Q^{-1}F(\omega)]\sqrt{1 - \frac{c^2}{c_0^2}[1 + Q^{-1}F(\omega)]^{-2}\sin^2\theta}}{c\,\cos\theta + c_0[1 + Q^{-1}F(\omega)]\sqrt{1 - \frac{c^2}{c_0^2}[1 + Q^{-1}F(\omega)]^{-2}\sin^2\theta}} \quad, \tag{1}$$

where

$$F = Q * \left(\frac{1 + \frac{i}{2}\ln(\frac{\omega}{\omega_0})}{1 + \frac{1}{Q\pi}\ln(\frac{\omega}{\omega_0})} - 1\right) \quad, \tag{2}$$

ω_0 is a reference frequency, θ is an angle of incidence, c_0 is the upper layer velocity, and c is the lower layer velocity. This expression assumes the nearly constant Q model of Aki and Richards (2002), as well as an acoustic upper layer. This expression can be expanded in terms of the small values $sin^2\theta$, and the perturbations

$$a_c = 1 - \frac{c_0^2}{c^2} \quad, \text{and}$$
$$a_Q = Q^{-1} \quad. \tag{3}$$

To second order in the perturbations and first in $sin^2\theta$, R can then be expressed as

$$R \approx \frac{1}{4}a_c(1 + \sin^2\theta) + a_c^2(\frac{1}{8} + \frac{1}{4}\sin^2\theta) - \frac{1}{2}a_c a_Q F_1(\omega)\sin^2\theta$$
$$-\frac{1}{2}a_Q F_2(\omega)(1 + \sin^2\theta) + a_Q^2 F_1^2(\omega)\left(\frac{1}{4} + \frac{3}{4}\sin^2\theta\right) \quad, \tag{4}$$

where
$$F_1(\omega) = \frac{i}{2} - \frac{1}{\pi}\ln(\frac{\omega}{\omega_0}) \quad, \tag{5}$$

and

$$F_2(\omega) = \frac{i}{2} - \frac{1}{\pi}\ln(\frac{\omega}{\omega_0}) + a_Q\left(\frac{-i}{2\pi}\ln(\frac{\omega}{\omega_0}) + \frac{1}{\pi^2}\ln^2(\frac{\omega}{\omega_0})\right) \quad. \tag{6}$$

As this expression is nonlinear in the perturbations, it cannot be solved for directly by least squares. A nonlinear expression for the reflection coefficient is given by

$$\mathbf{r} = \mathbf{Ga} \quad, \tag{7}$$

where

$$\mathbf{r} = \begin{bmatrix} R(\omega_1, \theta_1) \\ R(\omega_2, \theta_2) \\ \vdots \\ R(\omega_n, \theta_n) \end{bmatrix} \quad , \tag{8}$$

$$\mathbf{G} = \begin{bmatrix} \mathbf{g}_c & \mathbf{g}_Q \end{bmatrix} \quad , \tag{9}$$

$$\mathbf{g}_c = \begin{bmatrix} \frac{1}{4}(1 + \sin^2\theta_1) + a_c(\frac{1}{8} + \frac{1}{4}\sin^2\theta_1) - \frac{1}{4}a_Q F_1(\omega_1)\sin^2\theta_1 \\ \frac{1}{4}(1 + \sin^2\theta_2) + a_c(\frac{1}{8} + \frac{1}{4}\sin^2\theta_2) - \frac{1}{4}a_Q F_1(\omega_2)\sin^2\theta_2 \\ \vdots \\ \frac{1}{4}(1 + \sin^2\theta_n) + a_c(\frac{1}{8} + \frac{1}{4}\sin^2\theta_n) - \frac{1}{4}a_Q F_1(\omega_n)\sin^2\theta_n \end{bmatrix} \quad , \tag{10}$$

$$\mathbf{g}_Q = \begin{bmatrix} -\frac{1}{2}F_2(\omega_1)(1 + \sin^2\theta_1) + a_Q F_1^2(\omega_1)(\frac{1}{4} + \frac{3}{4}\sin^2\theta_1) - \frac{1}{4}F_1(\omega_1)a_c \\ -\frac{1}{2}F_2(\omega_2)(1 + \sin^2\theta_2) + a_Q F_1^2(\omega_2)(\frac{1}{4} + \frac{3}{4}\sin^2\theta_2) - \frac{1}{4}F_1(\omega_2)a_c \\ \vdots \\ -\frac{1}{2}F_2(\omega_n)(1 + \sin^2\theta_n) + a_Q F_1^2(\omega_n)(\frac{1}{4} + \frac{3}{4}\sin^2\theta_n) - \frac{1}{4}F_1(\omega_n)a_c \end{bmatrix} \quad , \tag{11}$$

and

$$\mathbf{a} = \begin{bmatrix} a_c \\ a_Q \end{bmatrix} \quad . \tag{12}$$

This expression can be solved for the perturbations by

$$\mathbf{a} = (\mathbf{G}^T\mathbf{G})^{-1}\mathbf{G}^T\mathbf{r} \quad . \tag{13}$$

Of course, we cannot directly solve this equation, as the matrix **G** is itself a function of the perturbation. If we solve this equation iteratively, however, we can create the matrix **G** using the perturbations solved for in the previous iteration. If the perturbations are small and we use an initial value of zero for these perturbations when first constructing **G**, we can expect that an iterative procedure will allow us to recover the perturbations accurately.

APPROXIMATING THE REAL PART OF THE REFLECTION COEFFICIENT

Our expression for R (Equation 1) is complex in general. In Equation 4, we can see that to second order in the perturbation terms, both the imaginary and real parts of R are functions of both frequency and incidence angle, as well as the velocity and attenuation perturbation terms. This means that given a measurement of the complex reflection coefficient, or its real or imaginary part, we should be able to invert for these perturbations. In real data acquisition, however, the inevitable noise and necessity of deconvolution of the source wavelet can mean that it is in practice quite difficult to accurately recover the full, complex reflectivity. A more easily attainable measurement is the amplitude spectrum of

the reflection coefficient, which is more robust to small noise and any phase-altering effects of the deconvolution. The amplitude spectrum of the reflection coefficient is given by

$$|R(\omega, \theta)| = \sqrt{\mathscr{R}[R(\omega, \theta)]^2 + \mathscr{I}[R(\omega, \theta)]^2} \quad , \tag{14}$$

which to first order in the perturbations is

$$|R(\omega, \theta)| \approx \sqrt{\left(\frac{1}{4}a_c(1 + \sin^2 \theta) - \frac{1}{2}a_Q\mathscr{R}(F_1(\omega))(1 + \sin^2 \theta)\right)^2 + \left(-\frac{1}{2}a_Q\mathscr{I}(F_1(\omega))(1 + \sin^2 \theta)\right)^2} \quad . \tag{15}$$

As pointed out by Bird (2012), if the term a_Q is much less than a_c, this equation simplifies to

$$|R(\omega, \theta)| \approx |\mathscr{R}[R(\omega, \theta)]| \quad . \tag{16}$$

This allows us to approach the problem treating the amplitude spectrum as the real part of the reflection coefficient. We can then solve for the perturbations through

$$\mathbf{a} = (\mathscr{R}(\mathbf{G}^T)\mathscr{R}(\mathbf{G}))^{-1}\mathscr{R}(\mathbf{G}^T)\mathscr{R}(\mathbf{R}) \quad . \tag{17}$$

While this approximation is valid for $a_Q << a_c$, we begin to face challenges as a_Q grows, or as we begin to consider higher order terms. At second order, for example, it is easy to see that in order to neglect the imaginary part of Equation 14, we require that $a_Q << a_c^2$. If this condition is not fulfilled, and we approach the problem using Equation 16, then using second and higher order terms will not improve our accuracy over the linear approximation.

In the case where a_Q is less than a_c, but not so much less that we can safely use Equation 16, we can iteratively update our approximation for $\mathscr{R}[R(\omega, \theta)]$ to attempt to gain more accuracy. This can be done by calculating some updated approximation,

$$|\mathscr{R}[R(\omega, \theta)]| \approx \sqrt{|R(\omega, \theta)|^2 - R_I^2} \quad , \tag{18}$$

where R_I is an approximation of the imaginary part of R, given, for example to second order by

$$R_I \approx -\frac{1}{2}a_c a_Q \mathscr{I}(F_1(\omega)) \sin^2 \theta - \frac{1}{2}a_Q \mathscr{I}(F_2(\omega))(1 + \sin^2 \theta) + a_Q^2 \mathscr{I}(F_1^2(\omega))\left(\frac{1}{4} + \frac{3}{4}\sin^2 \theta\right) \quad . \tag{19}$$

If the imaginary part of R is sufficiently small relative to the real part, R_I should converge to the imaginary part of the reflection coefficient, and Equation 18 should give a good estimate of the real part of the reflection coefficient.

SYNTHETIC EXAMPLES

In order to demonstrate the method described above, it was applied to synthetic data. To create the synthetic data, the exact reflection coefficient was first calculated for each angle and frequency. For each incidence angle, this reflectivity function was convolved with a delta function, to generate a reflection for that angle. Large amplitude random noise was
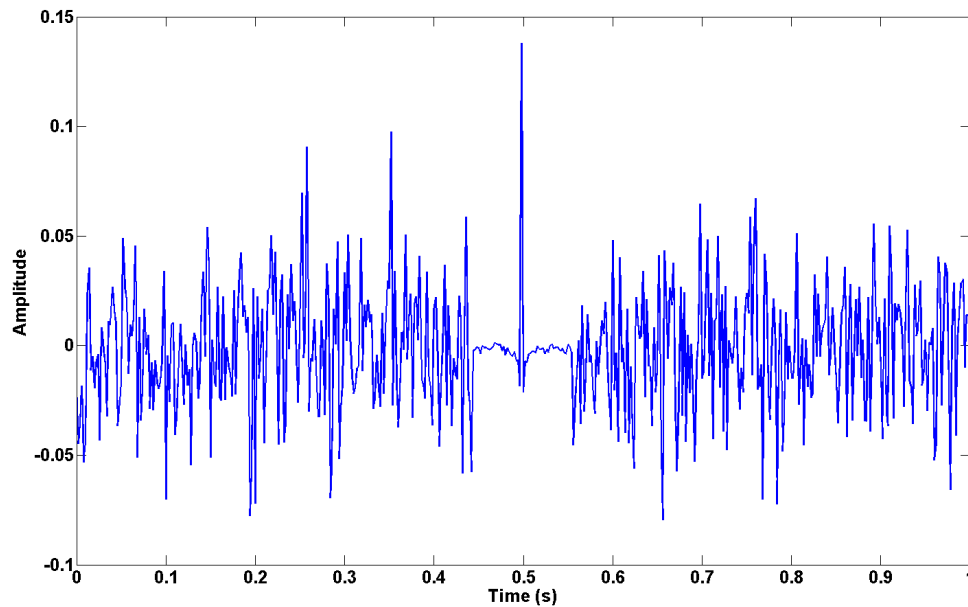
FIG. 1. One of the time series used as input. High amplitude noise is present far from the reflection, small amplitude noise near it. The reflection is at 0.5s.

then added the the time series outside of a small region near the reflection. This was done so that the use of some time-frequency transform other than the Fourier transform would be required, as it would when analyzing real data. Small amplitude noise was then added to the remaining region near the reflection, to introduce noise to the analysis. An example of a resulting trace from this method for one incidence angle is shown in Figure 1.

To be able to determine the frequency spectrum of the reflection alone rather than that of the whole trace, it is necessary to use some form of time-frequency analysis. In this example, the Gabor transform was chosen in preference to any progressive resolution time-frequency method due to the nature of the problem. So long as the time resolution is sufficient to separate the reflection of interest from other events, no further resolution is desirable, while provided this criterion is met we desire the maximum possible frequency resolution. The Gabor transform, with its frequency independent time and frequency resolution, best met these requirements. The Gabor transform of the signal in Figure 1 is shown in Figure 2. The frequency spectrum for the reflection recovered by the Gabor transform for one example is compared to the exact frequency spectrum in Figure 3.

Once an approximate frequency spectrum has been recovered, we can attempt to recover the velocity and attenuation of the lower layer by using Equation 17. Although we do not consider a wavelet in these examples, we limit the frequencies used to more accurately reflect real acquisition. In Figure 4, the result of a series of inversions done with low amplitude noise is shown. In this case, only a band from 30-80 Hz was used. Angles from 0-15 degrees were considered. It is evident in Figure 4 that the recovered values for Q are very accurate for most frequencies, and slightly better when using the second order terms in the inversion. Failure occurs at very small Q, and at large Q the noise seems to have a considerably greater effect. While using an iteratively approximated real reflectivity did not significantly improve the Q estimate (Figure 4), it did improve the velocity estimate
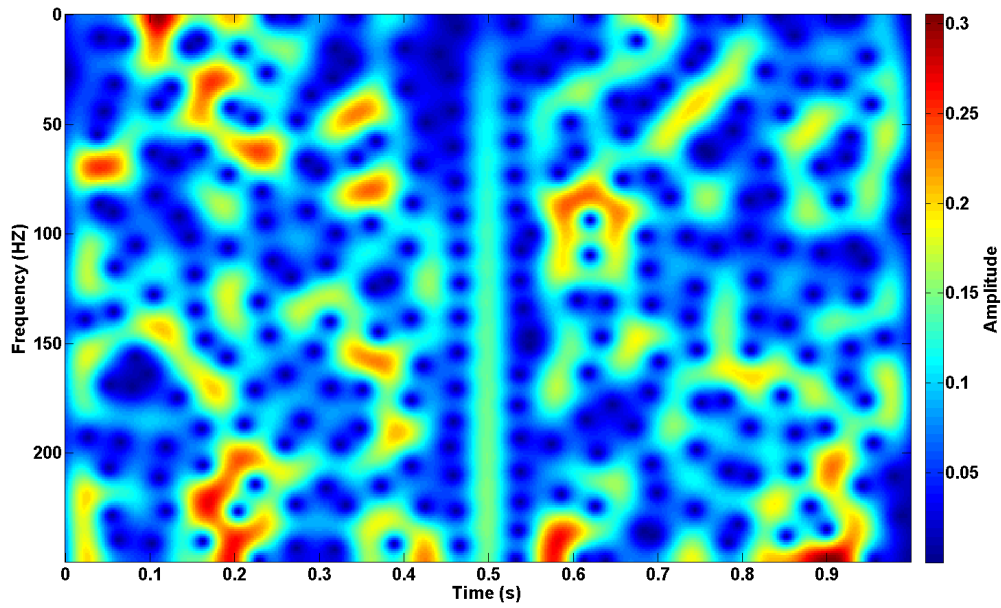
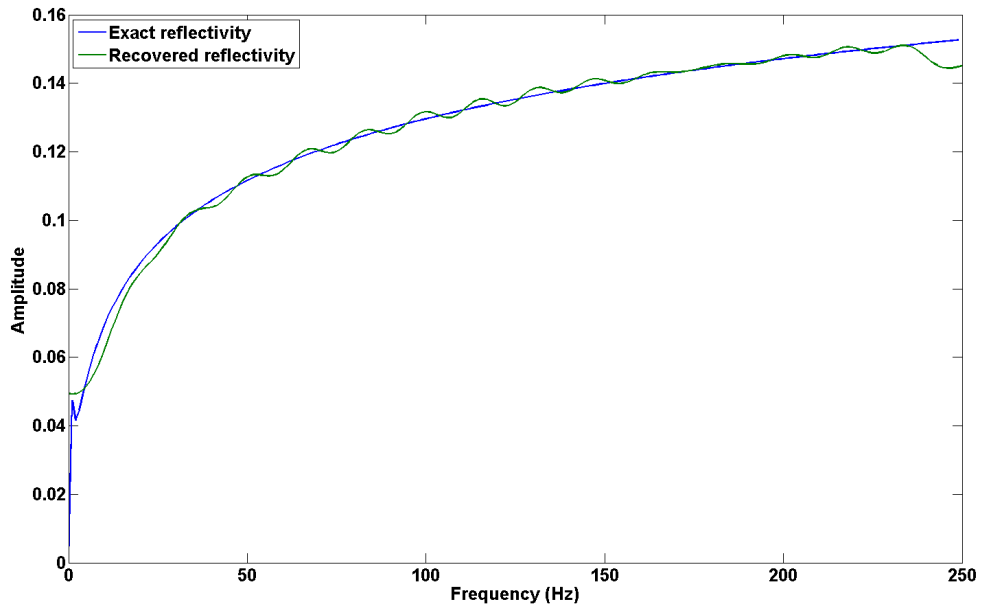FIG. 2. Gabor transform at zero incidence angle. The reflection is at 0.5s. In this case $Q = 6$.

FIG. 3. Comparison of reflectivity recovered by the Gabor transform (green) with the exact reflectivity (blue) for zero incidence angle, low noise and $Q = 6$.
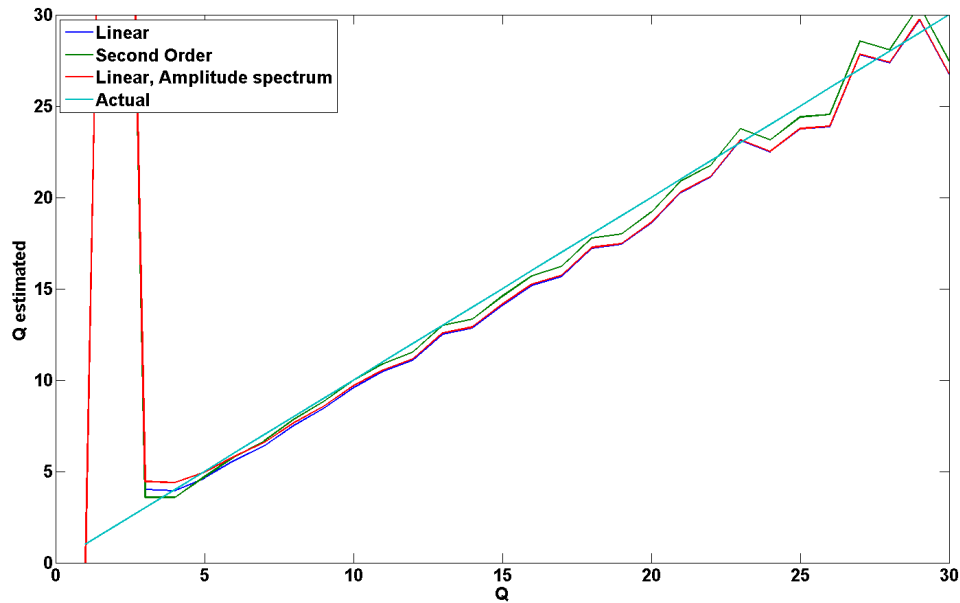
FIG. 4. Recovered Q using linear and second order approximations with approximate real reflectivity, as well as linear approximation where the amplitude spectrum is assumed to be equal to the real reflectivity. The second order approximation performs better, though failure occurs at very low Q, and large noise is present at large Q. $a_c = 0.4375$ in this example.

(Figure 5).

We might speculate that the failure at low Q in Figure 4 occurs due to either the large perturbation a_Q, or due to the failure of our assumption that the imaginary part of the reflection coefficient is less than the real part. The fact that the prediction is good at fairly low Q (say Q=5) and fails suddenly at lower Q (say Q=3) indicates that the latter is likely the case. To test this, we might repeat the experiment with a smaller velocity change. This should not change where failure occurs if the problem is a too large perturbation, while it will change where failure occurs if the problem is too large an imaginary part of the reflection coefficient. In Figure 6, the measurements are repeated with a smaller velocity perturbation. The result is a failure to recover Q at much greater Q values than in the previous example. This implies that the problem is indeed the size of the imaginary part of R in comparison to the real part, and not the size of a_Q. To further illustrate this point, Figures 7 and 8 show the approximation of the real part of the reflection coefficient used in the cases of $Q = 12$ and $Q = 7$ respectively. At $Q = 12$, where our result was good, our approximation of the real part of R was very close to the actual real value of R. In this case, the real part of R is greater than the imaginary part in the frequency band we used. In Figure 8, where $Q = 7$ however, the estimate of the real part of R is significantly different from the actual value. In this case the real part of R is smaller than the imaginary part for a large range of our used frequencies. This causes a major violation of our assumptions in Equation 18, thus making our Q estimation fail.

The noisy nature of the recovered Q at high Q in Figure 4 is somewhat surprising, as it is at high Q that the perturbation a_Q is smallest. In Figure 9, the result of a trial with much higher noise is shown. Here, the increased effect of noise at large Q is even more
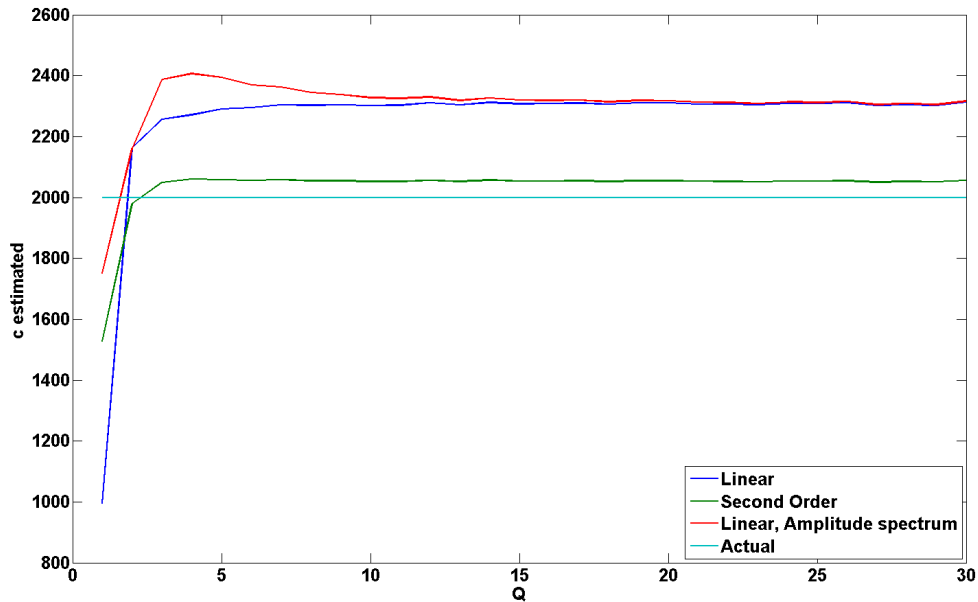
FIG. 5. Recovered velocity using linear and second order approximations with approximate real reflectivity, as well as linear approximation where the amplitude spectrum is assumed to be equal to the real reflectivity. The second order approximation far outperforms the linear approximations. $a_c = 0.4375$ in this example.
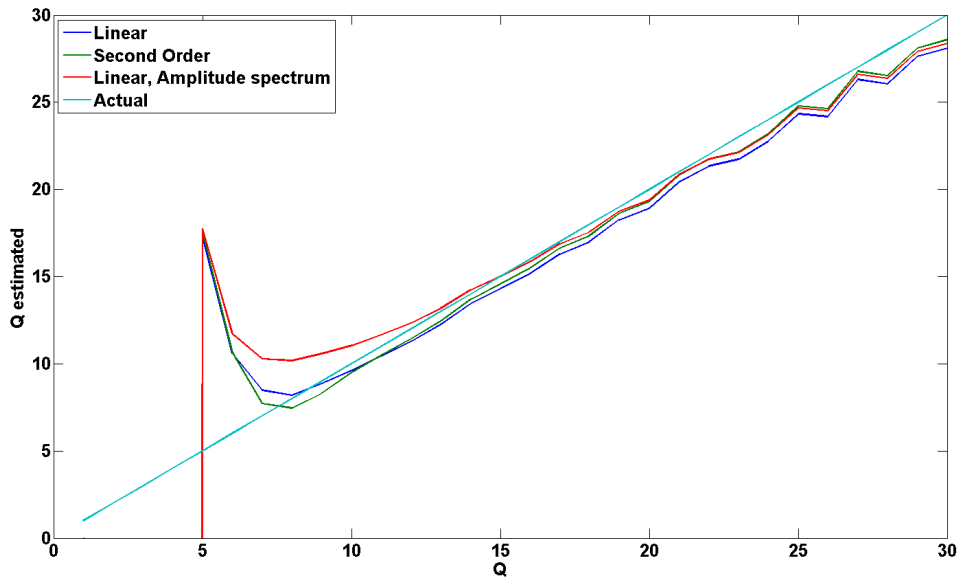

FIG. 6. Recovered velocity using linear and second order approximations with approximate real reflectivity, as well as linear approximation where the amplitude spectrum is assumed to be equal to the real reflectivity. $a_c = 0.2215$ in this example. The failure at larger Q than in Figure 4 implies that our assumption that the real part of the reflection coefficient is greater than the imaginary part is the cause of the error.
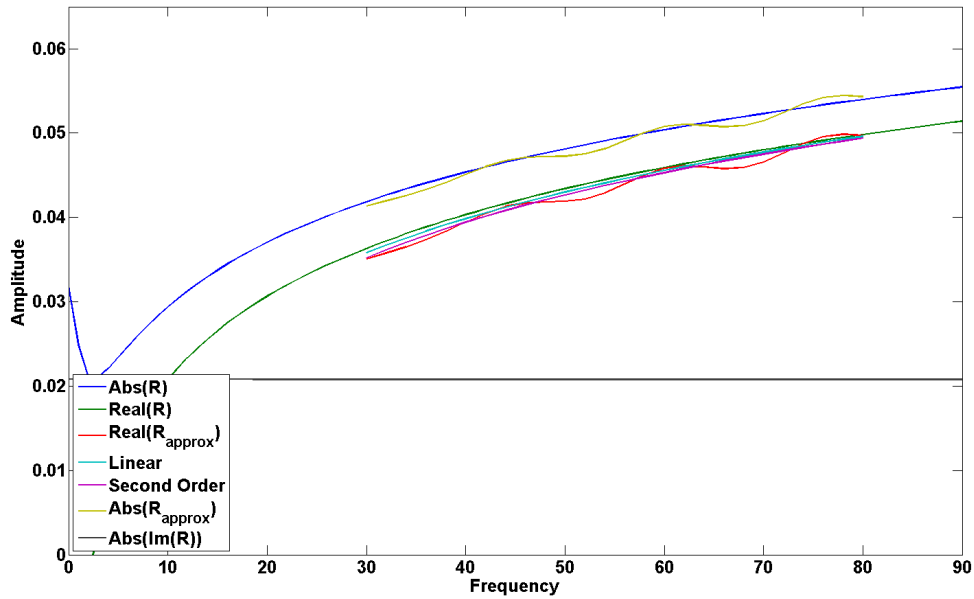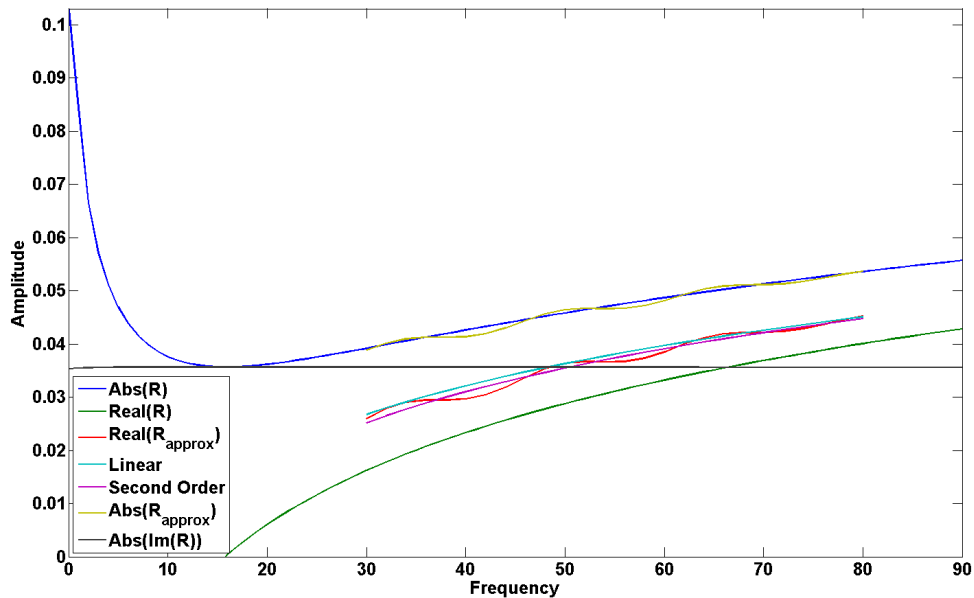
FIG. 7. Amplitude spectrum, as well as real and imaginary parts of the exact reflection coefficient, the spectrum recovered by the Gabor transform, the approximation of the real part of R, as well as the resulting fits for linear and second order inversion cases. This example is at normal incidence, but angles 0-15° were used to calculate the perturbations. The assumption of a small imaginary part is fulfilled, and the approximation of the real part is accurate. $Q = 12$ in this example.

FIG. 8. Amplitude spectrum, as well as real and imaginary parts of the exact reflection coefficient, the spectrum recovered by the Gabor transform, the approximation of the real part of R, as well as the resulting fits for linear and second order inversion cases. This example is at normal incidence, but angles 0-15° were used to calculate the perturbations. The assumption of a small imaginary part is badly violated, and so the approximation of the real part is inaccurate. $Q = 7$ in this example.
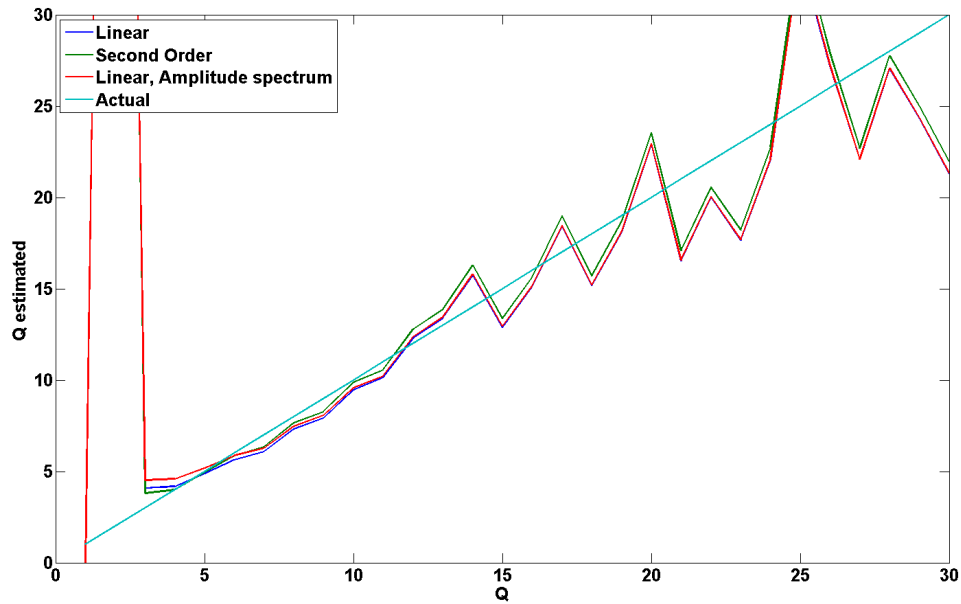
FIG. 9. Recovered Q using linear and second order approximations with approximate real reflectivity, as well as linear approximation where the amplitude spectrum is assumed to be equal to the real reflectivity. Larger amplitude noise than in Figure 4 is present. The effect of noise on the result is clearly greater at large Q. $a_c = 0.4375$ in this example.
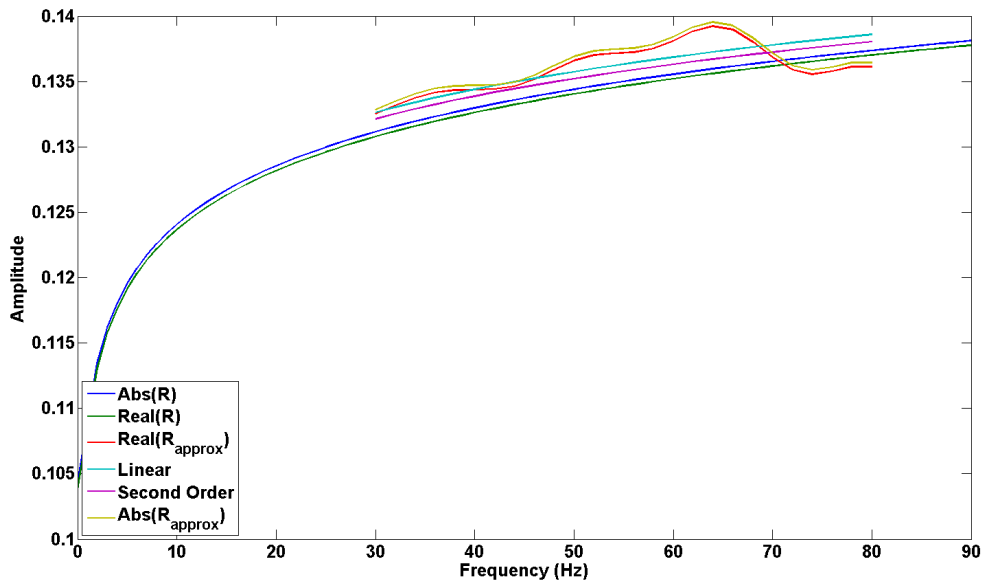

FIG. 10. Amplitude spectrum, as well as the real part of the exact reflection coefficient, the spectrum recovered by the Gabor transform, the approximation of the real part of R, as well as the resulting fits for linear and second order inversion cases. This example is at normal incidence, but angles 0-15° were used to calculate the perturbations. $Q = 25$ in this example. Large noise amplitudes cause large uncertainty in the relation between R and frequency.
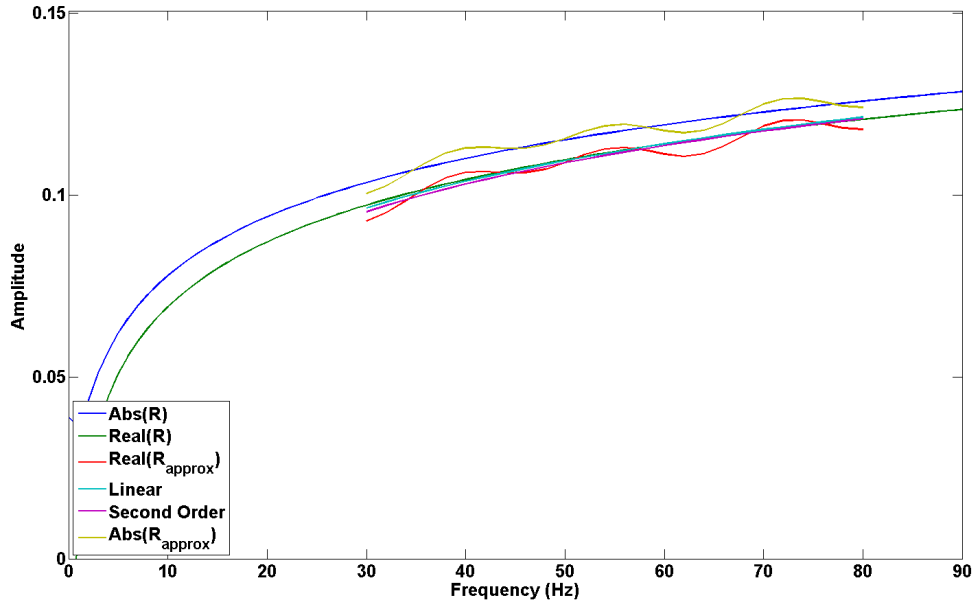
FIG. 11. Amplitude spectrum, as well as the real part of the exact reflection coefficient, the spectrum recovered by the Gabor transform, the approximation of the real part of R, as well as the resulting fits for linear and second order inversion cases. This example is at normal incidence, but angles 0-15° were used to calculate the perturbations. $Q = 7$ in this example. Noise amplitude is the same as in Figure 10, but is small relative to the change of R with frequency.
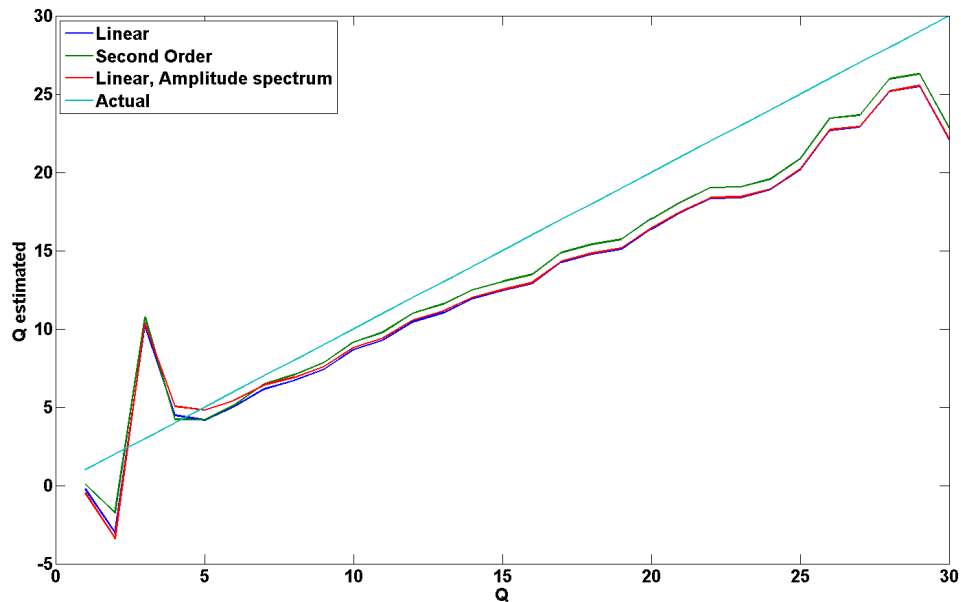

FIG. 12. Recovered Q using linear and second order approximations with approximate real reflectivity, as well as linear approximation where the amplitude spectrum is assumed to be equal to the real reflectivity. Noise is the same as in Figure 9, but the frequencies used are extended to 10-80 Hz, greatly reducing the effect of noise on large Q. An overall trend of underestimating Q is introduced, however, and increases with Q.
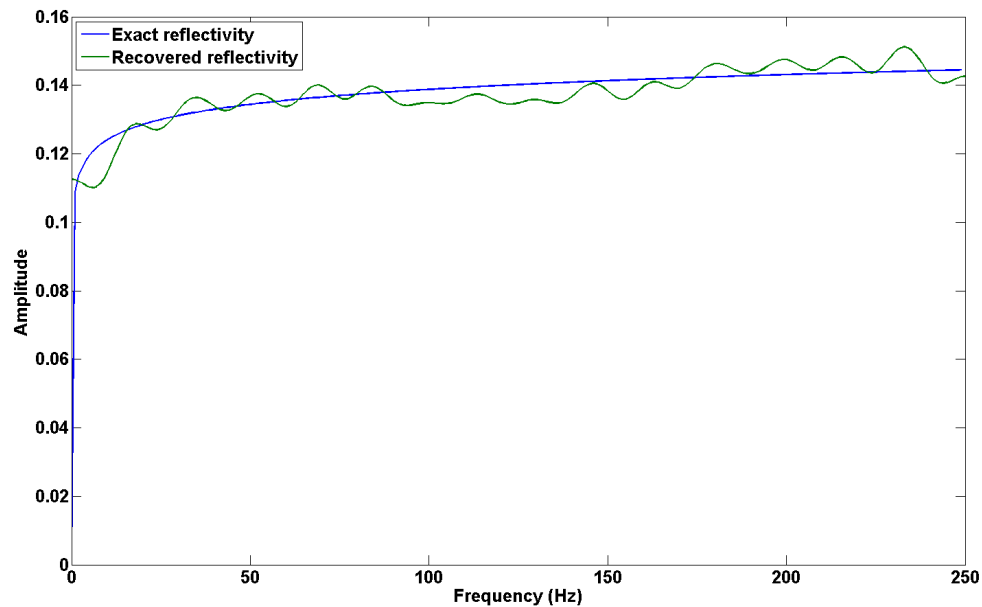
FIG. 13. Comparison of reflectivity recovered by the Gabor transform (green) with the exact reflectivity (blue) for zero incidence angle, low noise and $Q = 25$. Low frequencies are underestimated due to the uncertainty principle and the very low value for the zero frequency reflectivity. This problem is much more severe than for the small Q in Figure 3, where the change in reflectivity with frequency is not so severe at low frequencies.

pronounced. The reason for this behaviour is illustrated in Figures 10 and 11. In Figure 10, $Q = 25$, and we see an obvious source of error: in our frequency range of interest, the change in R with frequency is very small, and the random noise is sufficiently large to obfuscate the trend. This is why noise introduces such variability in the Q recovery at high Q. In Figure 11, the amount of noise is the same, but $Q = 7$, and the overall change of R with frequency is larger than the noise. This allows for accurate Q recovery. An obvious solution to the problem we encounter at large Q is to consider lower frequencies, where R changes rapidly with frequency for all Q. The problem with this approach is illustrated in Figure 12, where the same large noise as Figure 9 is used, but the frequency band used is increased to 10-80 Hz. It is evident in Figure 12 that we have significantly reduced the effect of random noise on the recovered Q at high Q, but in doing so we have introduced a significant systematic bias toward underestimating Q that increases with Q. This bias occurs due to the uncertainty principle. When we use time-frequency analysis to obtain the amplitude spectrum of just our reflection of interest, the temporal resolution we introduce comes at a cost to our frequency resolution. As the zero frequency reflection coefficient is typically much lower than the higher frequency reflection coefficients, this frequency uncertainty causes us to significantly underestimate our low frequencies. This problem is illustrated in Figure 13.

DISCUSSION

Failures at low Q are caused by violations of our assumption that the imaginary part of R is much less than the real part. This means that extension to higher orders in the perturbation are unlikely to give noticeable improvements. If inversion for lower Q is

desired, especially when the velocity change between layers is small, we need to address the problem introduced by this assumption. If only the amplitude spectrum of the reflection coefficient can be reliably obtained, this means that we may need to invert using the square of Equation 4, or some other formulation which avoids the assumption that either the real or imaginary parts of R to are small.

Noisy results at large Q are the result of large amplitude noise relative to the change in R with frequency. The best way to solve this problem seems to be introducing frequency ranges where R changes more rapidly with frequency, however this can result in using frequencies which due to the uncertainty principle are contaminated by very low frequency reflection coefficients. This means that our ability to recover high Q values depends both on the noise level, and the proximity of the reflection to nearby events, which will determine the temporal resolution required, and thus the achievable frequency resolution.

CONCLUSIONS

A second order, iterative least squares anacoustic inversion is shown to improve on linearized least squares approaches. Preliminary synthetic testing seems to show that this method works for a broad range of Q values, but fails at very large or very small values. Small Q failure was demonstrated to be systematic of a failure in our assumptions, and improved recovery here would require reliable measurement of the real part of the reflectivity, or a different formulation of the problem which avoids making these assumptions. Failure at large Q was shown to be more fundamentally rooted, and affected by the level of noise and the temporal resolution required to isolate the event of interest.

ACKNOWLEDGEMENTS

REFERENCES

Bird, C., 2012, Amplitude variation with frequency (avf) analysis of seismic data over anelastic targets: M.Sc. thesis, Univ. of Calgary.

Bird, C., Innanen, K., and Naghizadeh, M., 2011, Least squares avf inversion: CREWES Annual Report, **23**.

Castagna, J., Sun, S., and Siegfried, R., 2003, Instantaneous spectral analysis: Detection of low-frequency shadows associated with hydrocarbons: The Leading Edge, **22**, 120–127.

Innanen, K., 2011, Inversion of the seismic avf/ava signatures of highly attenuative targets: Geophysics, **76**, R1–R14.

Innanen, K., 2012, Anelastic avo approximations continued: CREWES Annual Report, **24**, 1–19.

Odebeatu, E., 2006, Application of spectral decompostion to detection of dispersion anomalies associated with gas saturation: The Leading Edge, **2**, 206–210.